EOPHYSICS, VOL. 60, NO. 3 (MAY-JUNE 1995); P. 667-681, 13 FIGS.

High-resolution crosswell imaging of a west Texas carbonate reservoir: Part l-Project summary and interpretation

Jerry M. Harris*, Richard C. Nolen-Hoeksema‡, Robert T. Langan**, Mark Van Schaack*, Spyros K. Lazaratos§, James W. Rector III‡‡

ABSTRACT

A carbon dioxide flood pilot is being conducted in a section of Chevron's McElroy field in Crane County, west Texas. Prior to CO_2 injection, two high-frequency crosswell seismic profiles were recorded to investigate the use of seismic profiling for high-resolution reservoir delineation and CO_2 monitoring. These preinjection profiles provide the baseline for time-lapse monitoring. Profile #1 was recorded between an injector well and an offset observation well at a nominal well-to-well distance of 184 ft (56 m). Profile #2 was recorded between a producing well and the observation well at a nominal distance of 600 ft (183 m). The combination of traveltime tomography and stacked CDP reflection amplitudes demonstrates how high-frequency crosswell seismic data can be used to image both large and small scale heterogeneity between wells: Transmission traveltime tomography is used to image the large scale velocity variations; CDP reflection imaging is then used to image smaller scale impedance heterogeneities. The resolution capability of crosswell data is clearly illustrated by an image of the Grayburg-San Andres angular unconformity, seen in both the P-wave and S-wave velocity tomograms and the reflection images. In addition to the imaging study, cores from an observation well were analyzed to support interpretation of the crosswell images and assess the feasibility of monitoring changes in CO_2 saturation. The results of this integrated study demonstrate (1) the use of crosswell seismic profiling to produce a high-resolution reservoir delineation and (2) the possibility for successful monitoring of CO_2 in carbonate reservoirs. The crosswell data were acquired with a piezoelectric source and a multilevel hydrophone array. Both profiles, nearly 80 000 seismic traces, were recorded in approximately 80 hours using a new acquisition technique of shooting on-the-fly. This paper presents the overall project summary and interpretation of the results from the near-offset profile.

INTRODUCTION

Chevron is conducting a miscible carbon dioxide pilot project in its McElroy field to evaluate the performance of a hybrid water-CO_2 injection process for improving oil recovery. Stanford University carried out a crosswell demonstration field experiment as part of a preinjection reservoir characterization study and to establish a baseline for subsequent CO_2 monitoring. Stanford's activities included acquisition of two crosswell seismic profiles, crosswell data processing, and the analysis and modeling of core samples to predict the seismic effects of CO_2. The crosswell profiles were acquired in mid-December, 1991. Profile #1 was recorded between the J. T. McElroy Well A (JTM-A) and J. T. McElroy Well B (JTM-B) at a nominal well-to-well distance of 184 ft (56 m). Profile #2 was run between JTM-A and JTM-C, with a nominal well-to-well distance of 600 ft (183 m) (See Figures la and lb.) In this paper, we summarize the main results from the near-offset Profile # 1.

Manuscript received by the Editor July 20, 1994.
*Stanford University, Geophysics Department, Stanford, CA 94305-2215.
‡Formerly with Stanford University; presently at 14 Homer Lane, Menlo Park, CA 940256320.
**Chevron Petroleum Technology Company, 1300 Beach Blvd., La Habra, CA 90631-6374; also at Geophysics Dept., Stanford University, Stanford, CA 943052215.
§Formerly Stanford University; presently with TomoSeis, Inc., 1650 W. Sam Houston Parkway, Houston, TX, 77043
#Formerly with Stanford University; presently with University of California, Berkely, CA, 94720

Two crosswell innovations were successfully tested during this study. The first was the acquisition method of shooting "on-the-fly," where the downhole source is fired at preset depth intervals as it moves continuously up the borehole. Stop-and-go methods of operating a downhole source are slow and totally inadequate for dense spatial sampling. The new on-the-fly method greatly improved depth control, permitted dense source spacing sufficient to avoid spatial aliasing of the high frequency signals, and provided an acquisition rate of over 1 000 traces per hour.

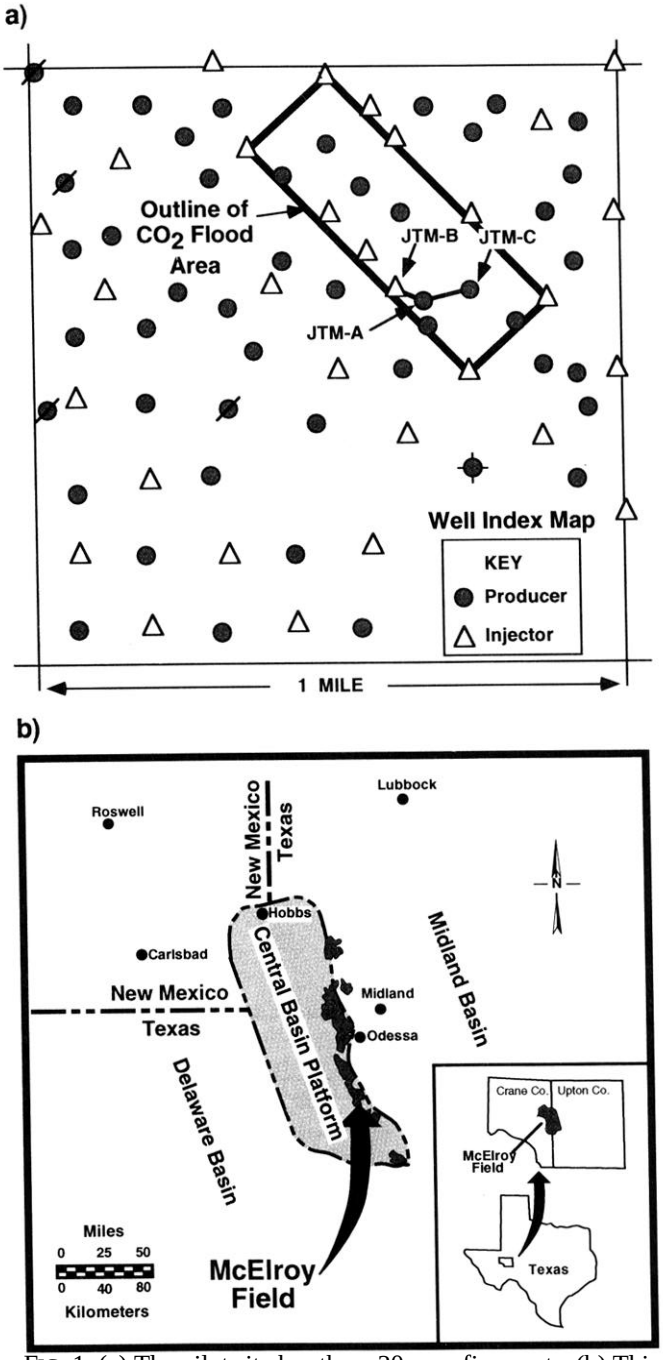

FIG. 1. (a) The pilot site has three 20-acre five spots. (b) This area map of the Permian Basin shows the location of the McElroy field on the eastern margin of the Central Basin Platform.

With this method, the 40,000 trace near-offset profile was recorded in a little more than 40 hours, some five to 10 times faster than previously demonstrated. The second innovation was the implementation of true "well-to-well" reflection imaging on a field dataset. Prior to this work, high-resolution reflection imaging from crosswell data had been demonstrated only in the vicinity of the wellbore, never all the way from one well to the other (Lazaratos et al., this issue). The type of reflection imaging used in this study is similar to processing over 1 500 offset VSPs. Because of the complexity of the wavefield, new methods of wavefield separation were developed to enhance primary reflections prior to imaging (Rector et al., this issue). The resulting crosswell reflection images provide vertical resolution approaching one-half wavelength, approximately IO ft for the P-waves and 5 ft for the S-waves. The success of the reflection imaging is intimately related to data quality, and therefore the acquisition method of on-the-fly source operation.

The research to date on Profile #1 is reported in five papers, presented together as a case study on imaging a west Texas carbonate reservoir: This paper (Part 1) provides a description of the site, reservoir geology, a summary of data acquisition and tomographic data processing, a brief summary of the core analysis, and an interpretation of the results. Part 2 presents the results of a full wavefield analysis and modeling study used to identify the plethora of wave modes observed in the data; Part 3 presents the detailed processing steps employed in separating primary *P-wave* and S-wave reflections from the complicated full seismic wavefield; Part 4 presents the results of high-resolution crosswell reflection imaging of both *P-waves* and S-waves; and finally, Part 5 summarizes the analysis of laboratory core measurements and the development of a rock properties model that is used to predict the seismic visibility of CO_2.

RESERVOIR GEOLOGY AND SITE DESCRIPTION

The McElroy field is located on the eastern margin of the Central Basin Platform in Crane and Upton Counties, Texas (Harris et al., 1984; Ward et al., 1986). The locations of the pilot site and the field are shown in Figures la and lb. The geological structure is a N-NW trending, asymmetric anticline that has a steeply dipping eastern limb, a gently dipping western limb, and provides about 250 ft (76 m) of structural closure. The reservoir is a stratigraphic-structural trap with oil production coming primarily from the shelf dolomites of the Grayburg formation. Terrigenous sediments and evaporites, known in this area as the Lower Queen formation, provide a cap and seal for the Grayburg reservoir rocks. The Grayburg is deposited unconformably above the San Andres, a formation of evaporitic dolomites. The field has been producing oil since the mid-1930s.

The reservoir is approximately 2,900 ft (884 m) deep. Oil production comes from a gross pay zone with an average thickness of approximately 275 ft (84 m). Overall, the reservoir is characterized by irregular geometry and significant spatial variations in both porosity and permeability. Average porosity is about 10% but varies higher because of solution enhancement and lower because of secondary deposition of evaporites. Permeability is also quite variable throughout the field, averaging only a few millidarcies in the

main pay, but increasing to a few hundred millidarcies in thin high permeability streaks, which can cause significant fluid channeling. As a result of this heterogeneity, oil recovery varies dramatically across the field, with the highest production coming from the central area and lowest from the flanks. The lower recovery in the flanking areas results from low reservoir quality (e.g., low permeabilities, high water saturations). Up dip to the west, porosity and reservoir quality decrease because pore space is filled with evaporite minerals. Down dip to the east, reservoir quality decreases because of high water saturation as the oil-water contact is approached.

The CO_2-injection pilot project is being conducted in Section 205, in the southwest portion of the field (Lemen et al., 1990). The top of the Grayburg formation occurs at a depth of about 2,750 ft (838 m) and the top of the San Andres at about 3,040 ft (927 m). (See Figure 2.) Within the Grayburg, zones E, D5, and M are all reservoir units, though the principal "pay zone" is the D5; their tops, indicated by electric-log markers, occur at about 2750 ft (838 m), 2,860 ft (872 m), and 2,950 ft (899 m), respectively. In the pilot section of the field, porosity, permeability and, consequently, reservoir quality generally increase from west to east. However, these trends mask the high spatial variability of the reservoir and the lack of spatial correlation between porosity and permeability (Lemen et al., 1990).

Seismic Properties

Seismic properties of the formations are approximately known from a suite of logs taken in 1991 from the observation well, together with earlier logs taken from other wells throughout the field. The available logs for JTM-A and JTM-B, plotted in Figure 2, express a near layer-cake geology. Although the structure is simple, Lemen et al. (1990) highlight the difficulty with correlating reservoir zones from well to well. One purpose of the crosswell experiment is to attempt interwell delineation of the reservoir, thus providing essential information for stratigraphic correlation. Compressional wave velocities range from about 14,000 ft/s (4,267 m/s) to over 21,000 ft/s (6,400 m/s). Shear velocities range from approximately 8000 ft/s (2,440 m/s) to nearly 12,000 ft/s (3,660 m/s), and are approximately (though not uniformly) 1.8 times less than the compressional velocities. Unfortunately, a measured shear log is available only at the observation well JTM-A. To estimate the shear velocity at the injector, we calculated the V_p/V_s ratio from JTM-A and applied this ratio to measured V_p from JTM-B. Density values range from slightly less than 2.6 gm/cm^3 in the reservoir to over 3.0 gm/cm^3 elsewhere. The thickness of the D5 pay zone (~100 ft or 30 m) and its large seismic contrast to the surrounding formations (>20%) create an easily visible target for both transmission tomography and reflection imaging.

Well Descriptions

The CO_2 study area is part of three 20-acre five spot patterns. The initial crosswell study involves three wells in the study area, JTM-A, JTM-B, and JTM-C (Figure 3). Two of these, JTM-B and JTM-C, were drilled in 1988 as in-fill wells for waterflood realignment (Lemen et al., 1990). JTM-B was drilled as an injector and JTM-C as a producer. In 1991, Chevron drilled JTM-A as an observation well for the CO_2 pilot project. It was drilled to a depth of 3260 ft (994 m) and a total of 285 ft (87 m) of 3.25-inch (8.3 cm) diameter, unoriented core was cut between 2,775 ft (846 m) and 3,060 ft (933 m). The observation well was cased through the production zone in fiberglass to permit monitor logging.

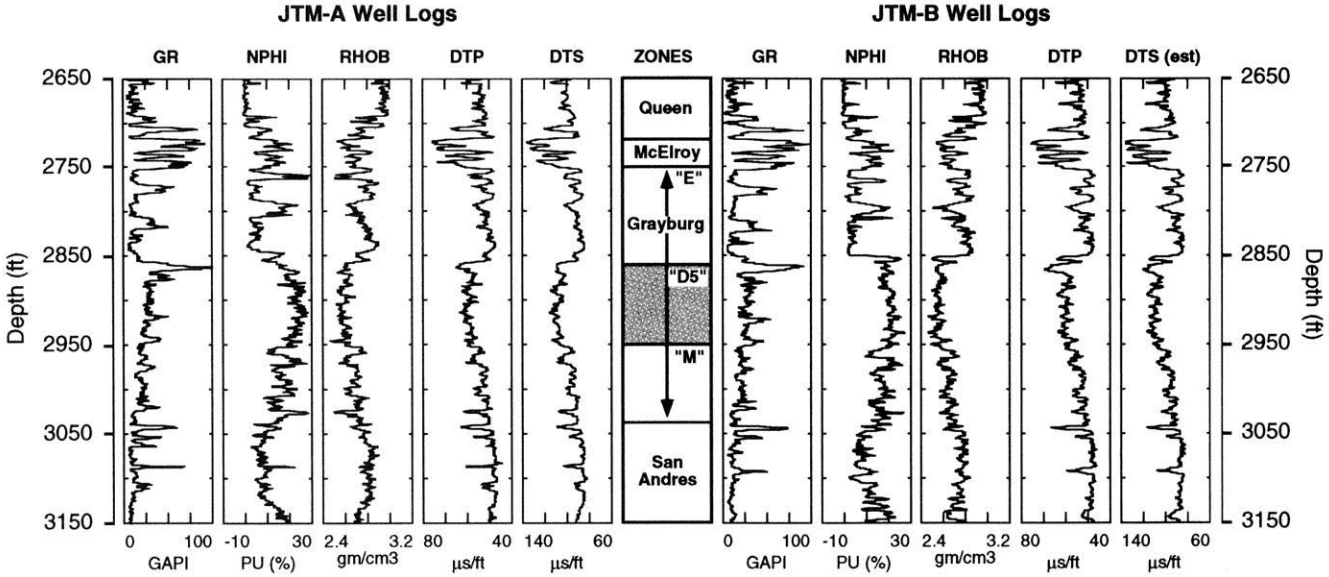

FIG. 2. The suite of well logs (gamma ray, neutron porosity, density, sonic-DTP, and sonic-DTS) for JTM-A and JTM-B illustrates the near layer-cake geology. The wells are nominally 184 ft (56 m) apart at reservoir depths. The shear wave log for JTM-B was estimated using the V_p/V_s ratio calculated from the JTM-A sonic. The "zones" column delineates approximately 300 ft (100 m) of reservoir quality rocks, i.e., the Grayburg formation. Production is from the "D5" zone.

DATA ACQUISITION

The two crosswell profiles were run in December 1991, prior to injection of CO_2. The first was taken between the observation well JTM-A and the injector JTM-B, the second between JTM-A and the producer JTM-C. Nearly 80 000 traces were recorded in a little more than 80 hours. Prior to these surveys, no previous crosswell experiment had accomplished such high data rates. Source and receiver positions were uniformly sampled at 2.5 ft (0.8 m) over a vertical aperture of roughly 500 ft (152 m) in Profile #1. Because of the larger well spacing, Profile #2 was recorded with a larger vertical aperture but coarser source and receiver spacing, i.e., 5 ft (1.5 m). The aperture geometry of each survey is illustrated in Figure 3. The source and receiver systems and their operation are described in the next section.

The Acquisition System

A schematic outline of the acquisition system is illustrated in Figure 4. The system, designed at Stanford University, consists of a piezoelectric downhole source, a six-level hydrophone array, and two wireline logging trucks with associated instrumentation to control the downhole tools. Both source and receiver are run on 7-conductor oil field wirelines. Field operations are directed from the source truck where instruments for source and receiver are located. The system is highly automated. Tool depths are monitored electronically and recorded to the SEG-Y header along with

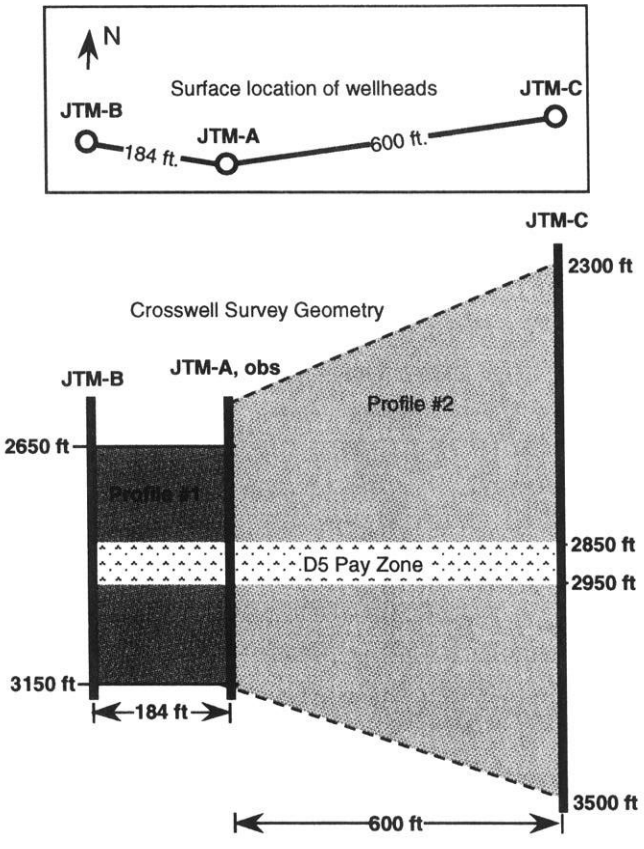

FIG. 3. Two crosswell profiles were acquired in December, 1991. Profile #1 (201 sources x 178 receivers) was recorded between JTM-A and JTM-B. Profile #2 (240 sources x 153 receivers) was recorded between JTM-A and JTM-C. Receivers are in JTM-A for both. The JTM-A was drilled in 1991 as an observation well for the CO_2 pilot study. JTM-B (injector) and JTM-C (producer) were drilled in 1988 as part of the waterflood realignment.

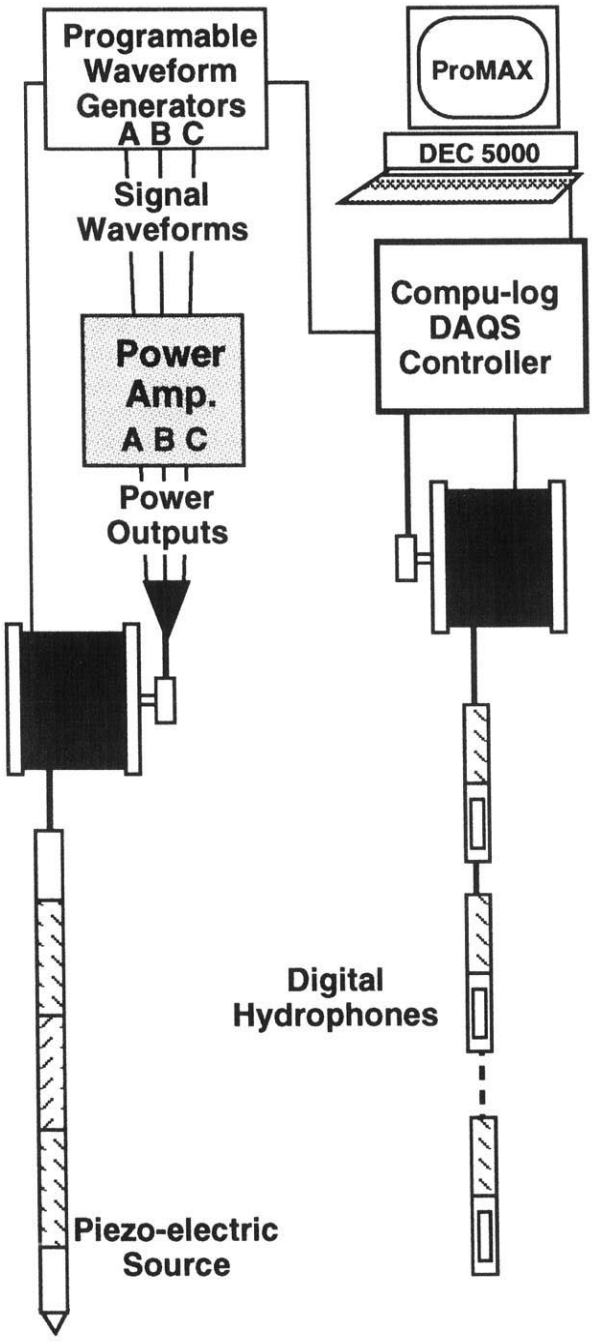

FIG. 4. This schematic diagram illustrates the major parts of Stanford's crosswell data acquisition system. The system consists of a 3-element piezoelectric source and a multilevel downhole digital array of hydrophones. The source is fired while moving at 400-1000 ft/hr (122-305 m/hr), i.e., on-the-fly. Data are analyzed in the field using ProMAX®, Advance Geophysical Corporation's interactive processing system.

the trace data. Demultiplexed seismic data are transferred to a UNIX workstation for correlation, in-field quality control, and processing.

The source consists of three cylindrical piezoelectric elements. These elements are placed in the sonde to form a symmetric source structure. Symmetry reduces spurious modes of vibration, thus providing more power to the desired monopole mode. Two banks of power transformers, mounted above and below the transducers, maintain this symmetry. The source transducers are wired to form an "adjacent array." That is, the elements of the source are capable of being operated independently for time-domain beam steering, or may be driven as three independent sources simultaneously fired (i.e., coded) at different depth levels, or simply operated in parallel as a single distributed source. Signal waveforms are produced by three 12-bit D-to-A phase-coherent arbitrary waveform generators. A variety of waveforms, including sweeps, pulses, and pulse sequences may be used. The source array is powered by a three-channel 24 kVA linear power amplifier. Power is delivered via 12,000 ft (3,658 m) of 0.579-inch diameter 7-conductor armored wireline. The cable has the standard 7-conductor armored configuration but uses larger conductors and special insulation for better power transfer and higher voltage operation. When beam steering is not required, a single conductor wireline may be used. For this profile, the transducers were wired in parallel to form the simple monopole source.

The receiver system consists of a six-element hydrophone array. Each element is independently digitized downhole to 16 bits. To reduce transmission throughput and- increase acquisition speed, data are stacked downhole and double buffered to permit simultaneous stacking and transmission. The hydrophones are interfaced to the surface via a downhole telemetry sonde that controls communications and data transfer. A surface computer provides surface control of downhole recording parameters, e.g., sampling rate, analog and digital gains, stacking depth, and high- and low-pass filter settings, and records the demultiplexed trace data and recording parameters to tape in SEG-Y format. The system is operated on 17,000 ft (5182 m) of 'jr-conductor wireline.

Field Operations & Acquisition Parameters

Prior to this study, high-frequency crosswell datasets had been recorded only for traveltime tomography and because of spatial aliasing were not suitable for reflection processing (Rector et al., this issue). Although difficulties in wavefield decomposition as a result of spatial aliasing had been demonstrated (Harris, 1988), the expense of adequate dense sampling had been prohibitive because of slow recording speed. Shooting on-the-fly addresses the speed problem and therefore the sampling problem. The technique significantly improves depth positioning because the constant movement of the source under steady wireline tension provides uniform spacing between shot points. Sampling uniformity can be accurately maintained throughout the entire survey. In addition to increasing acquisition speed and providing dense shot spacing, shooting on-the-fly greatly reduces human interaction, thereby reducing human errors and improving overall data quality. Less than 1% of the recorded traces in Profile #1 were lost because of computer malfunction or operator error. Although the receiver array could not be operated on-the-fly because of motion-generated noise, commonly used wireline procedures were employed to maintain receiver depth accuracy. As a result, overall depth control for the profile is excellent in both source and receiver wells.

The data are recorded as common-receiver gathers or fans. For each fan the hydrophone array is positioned and the source scanned up the well at a rate between about 400 and 1000 ft/hr (122-305 m/hr). As the source moves, the depth system triggers the acquisition system to fire the source and stack a specified number of sweeps at programmed depth intervals, i.e., every 2.5 ft (0.8 m) for this profile. Following the completion of a source scan, the receivers are repositioned (first lowered then pulled up) and the source scan repeated. The number of stacks is determined by the desired signal-to-noise ratio and acquisition speed. The depth interval over which the stack is made, i.e., shot point smear, is influenced by the scan rate of the source and the number of stacks. Shot point smear in Profile #1 is insignificant, approximately 2.5 inches.

The data in Profile #1 were collected over the depth interval 2650 ft to 3150 ft (808-960 m). After editing, the profile contained approximately 36 000 traces: 178 receiver points and 201 shot points. A vertical stack of two records was taken with a sweep waveform of 250 to 2000 Hz in 200 ms. The records were sampled at 100 microseconds with low-cut filters set to 250 Hz and the high-cut filters at 2000 Hz. A representative common-receiver gather from Profile #1 and its average frequency spectrum are shown in Figures 5a and 5b. Energy with signal-to-noise greater than 60 dB can be seen over the entire range of sweep frequencies. Moreover, we see from Figure 5a that the data are rich in modal arrivals, including, direct P-waves, direct S-waves, *P-S* and *S-P* conversions, *P* head waves, guided waves, primary and multiple *P* and S reflections. Van Schaack et al. (this issue) discuss wavefield modeling, decomposition, and identification of the various modes.

DATA PROCESSING

Our data processing strategy incorporates both traveltime tomography and reflection imaging to generate images of the interwell region. The philosophy is to use traveltime tomography to generate a "low" resolution and quantitatively accurate image of inter-well velocity, then reflection imaging to generate a "high" resolution, though qualitative, image of interwell structure. Following data editing and the specification of the wellbore geometries, the first processing step is to pick traveltimes and estimate a velocity model using transmission traveltime tomography. This velocity model is then used for ray tracing and CDP mapping of reflections. Prior to reflection imaging, however, the waveform data are analyzed and filtered to enhance primary reflections, a process called wavefield separation. Traveltime tomography is discussed below. More detailed descriptions of the wavefield separation and reflection processing are presented in Rector et al. (this issue) and Lazaratos et al. (this issue), respectively.

Traveltime Processing

Picking nearly 40 000 P-wave traveltimes by hand may seem a daunting task; nevertheless, it was accomplished in about three hours using commercial picking software. The general picking philosophy for the P-waves was to pick first-arriving energy without discriminating between direct waves and head waves. For shear waves, however, the fluid coupled source and receiver do not permit strong detection of shear energy near zero vertical offsets (Van Schaack et al., this issue). S-wave picks at these near horizontal angles were obtained by using the P-wave picks as a guide (actually 1.8 times the P-wave picks) and editing the estimates to fit the barely visible S-wave waveforms. The resulting P-wave and S-wave picks are shown in Figures 6a and 6b, respectively. The difference in traveltime (dynamic range (ratio of largest traveltime to the smallest) is indicative of varying Poisson ratio over the interval. P-wave traveltimes have a dynamic range of approximately 4, whereas the shear wave range is closer to 3.5.

The picks were inverted by the STRINGS method (Harris et al., 1990). The STRINGS algorithm uses initial value ray tracing and a SIRT solver to estimate a correction to an assumed starting velocity model. The starting velocity is then updated by the small SIRT-generated perturbation and

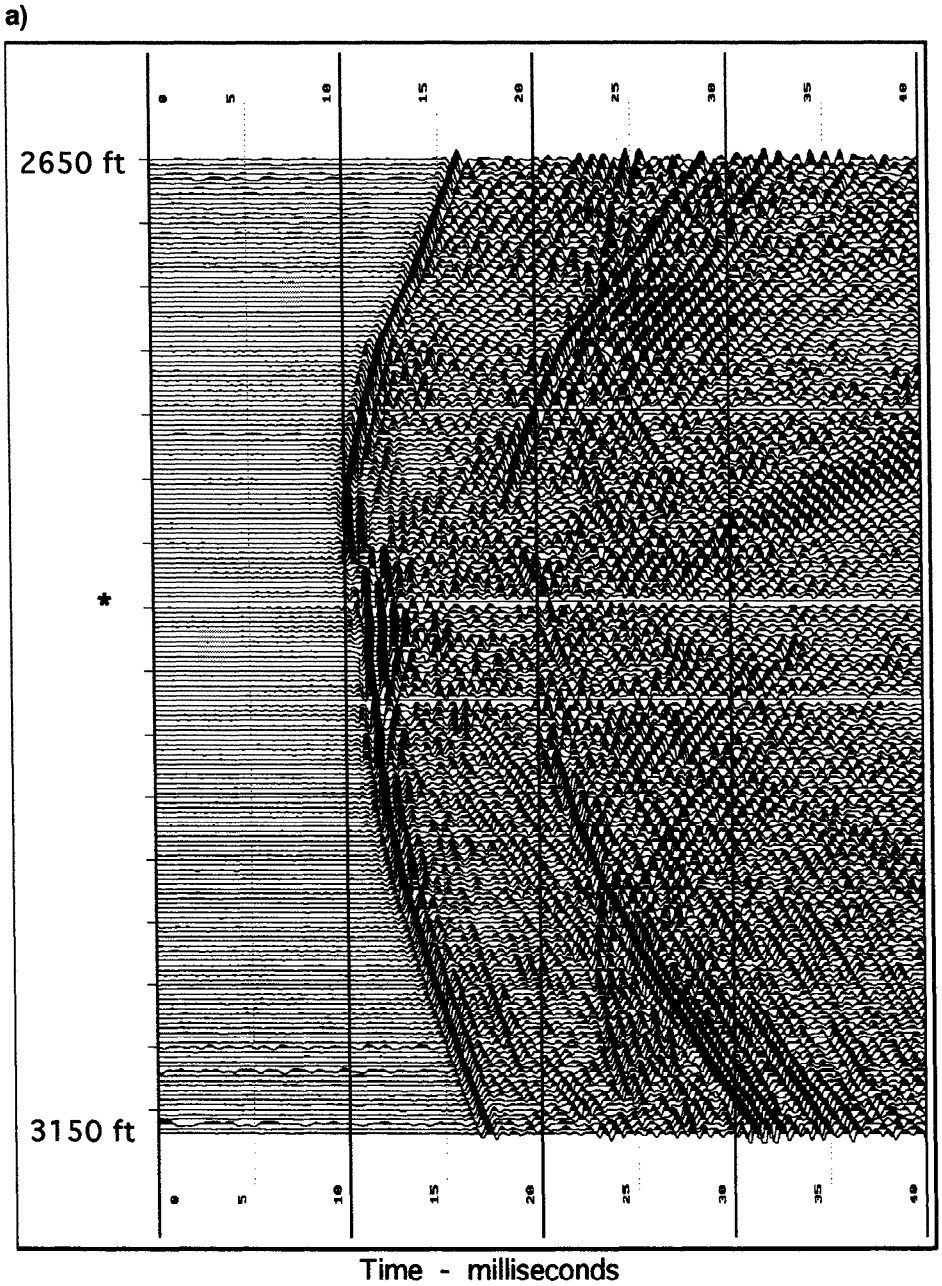

FIG. 5. This common-receiver gather from Profile #1 was recorded for a hydrophone located at 2880 ft (878 m) (marked *). Six or more gathers of this type were recorded simultaneously and required little more than 30 minutes to acquire with the on-the-fly source scan. (a) The gather contains 201 source points spaced 2.5 ft (0.8 m) apart from 3150 ft (960 m) to 2650 ft (808 m); (b) The average frequency content follows the sweep, e.g., 250-2000 Hz.

used as a new starting model for the next iteration. The process is continued for several iterations until the average absolute value of the traveltime residuals reach an acceptably low value. The rate of convergence is affected by a number of user-defined variables: the starting model, pixel size, smoothing, number of rays used, number of SIRT backprojections, angular aperture, and the step-size used in ray tracing. However, the final result appears not to be significantly affected by these parameter choices. A very important consideration, however, is the correction for well deviation. In this study, well deviation is handled by creating a depth-local 2-D coordinate system, i.e., ribbon coordinates. The ribbon rotates or twists slowly with depth to account for local well deviation. Ribbon coordinates retain the true source-receiver spacing but allow distortion of the image plane to match a slowly, changing borehole geometry. In the ribbon coordinate system, the lateral coordinate displayed in the tomograms is read as the radial distance in the direction of one well from the other well at that depth.

The predominant 1-D structure of the geology can be seen in the geometric patterns of the picks (Figures 6a and 6b), in this case as reflection symmetry about the main diagonal where shot depth equals receiver depth. This observation and the simple geological structure of our site suggests that we first invert for a 1-D velocity model. The 1-D inversion is accomplished by adjusting the horizontal pixel dimensions in STRINGS to equal the well spacing. Starting from a constant velocity background model, four ray trace iterations with a total of 40 SIRT backprojections were run, resulting in the P-wave and S-wave velocity tomograms presented in Figures 7a and 7b, respectively. These I-D tomograms were then used as starting models for 2-D inversion, again using STRINGS though in this case with the pixel size decreased to a 2 ft by 2 ft (0.6 m by 0.6 m) square. The final 2-D tomograms are given in Figures 8a and 8b, for P-wave velocity and S-wave velocity, respectively. The rates of convergence for the combined 1-D and 2-D iterations are presented in Figure 9. The final average absolute residual traveltime error is approximately 20 microseconds for the P-waves and approximately 50 microseconds for the S-waves. Interpretation of the tomograms is discussed in the section below. Next, we briefly review the method of reflection processing.

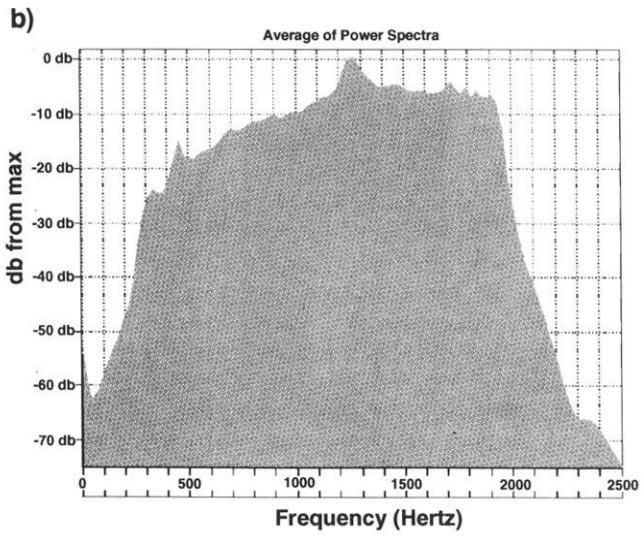

FIG. 5. (continued)

Reflection Processing

The method used for reflection imaging is often called VSP-CDP mapping. The general procedure for crosswell data is similar to processing multiple offset VSPs, though the details are very different, especially the essential step of wavefield separation. The data are first separated into upgoing and downgoing waves, then filtered to enhance primary reflections. Normal moveout mapping trajectories are then calculated from a velocity model derived from the tomogram. The separated common-source and common-receiver gathers are then mapped along the trajectories to create interwell reflection images, i.e., of impedance contrasts. The final image is generated by stacking individually mapped common-source, common-receiver, upgoing and downgoing gathers. For the near-offset profile under discussion, each stacked P-wave and S-wave reflection image is equivalent to

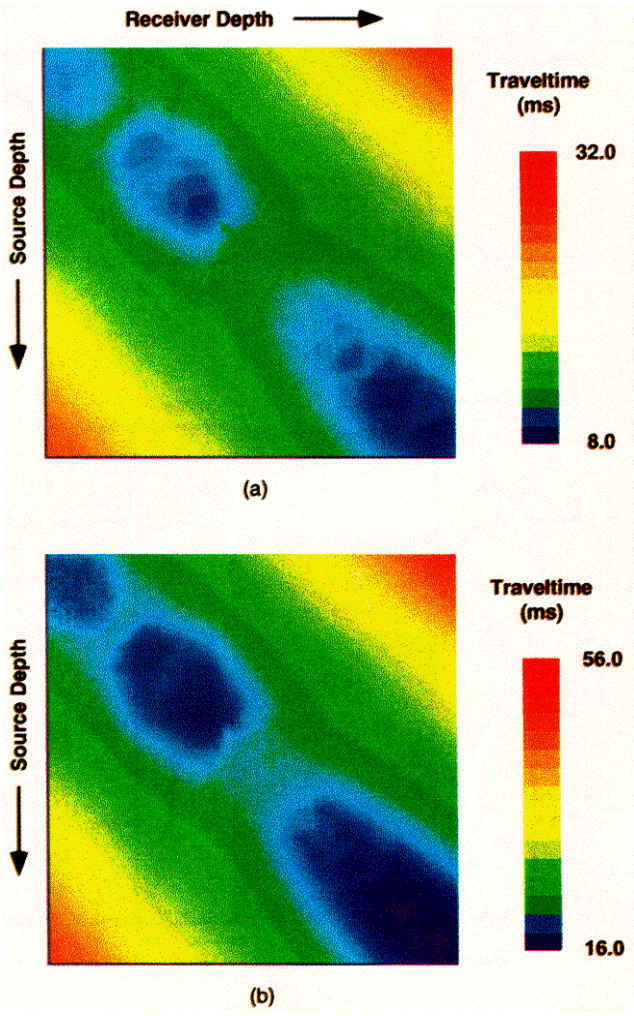

FIG. 6. The transmission traveltimes used in tomography are displayed as source-receiver pick images: (a) P-wave picks from the field dataset; (b) S-wave picks from the field dataset. The 1-D nature of the geology is seen in the reflection symmetry about the main diagonal.

approximately 750 single-fold, VSPs. This description of the procedure could be simply called "map and stack." However, such a simple description would not convey the complexity and sensitivity of the procedure to the details. In fact, as discussed in detail by Lazaratos et al. (this issue), a simple map and stack strategy does not lead to very good results because of the large variations in signal-to-noise throughout the section. The final stacked P-to-P and S-to-S reflection images are shown in Figures 10a and 10b, respectively. Their interpretation is discussed below.

INTERPRETATION

As stated in the Introduction, the principal objective of the crosswell experiment was to examine the potential of crosswell seismic profiling for reservoir delineation prior to CO_2 injection. Lemen et al. (1990) emphasize the difficulty in correlating individual layers from one well to another from log data alone. It was anticipated that crosswell profiling would provide a direct sampling of inter-well heterogeneity at a scale potentially useful in bridging the gap between logs and surface seismic profiling. In this section, we present a

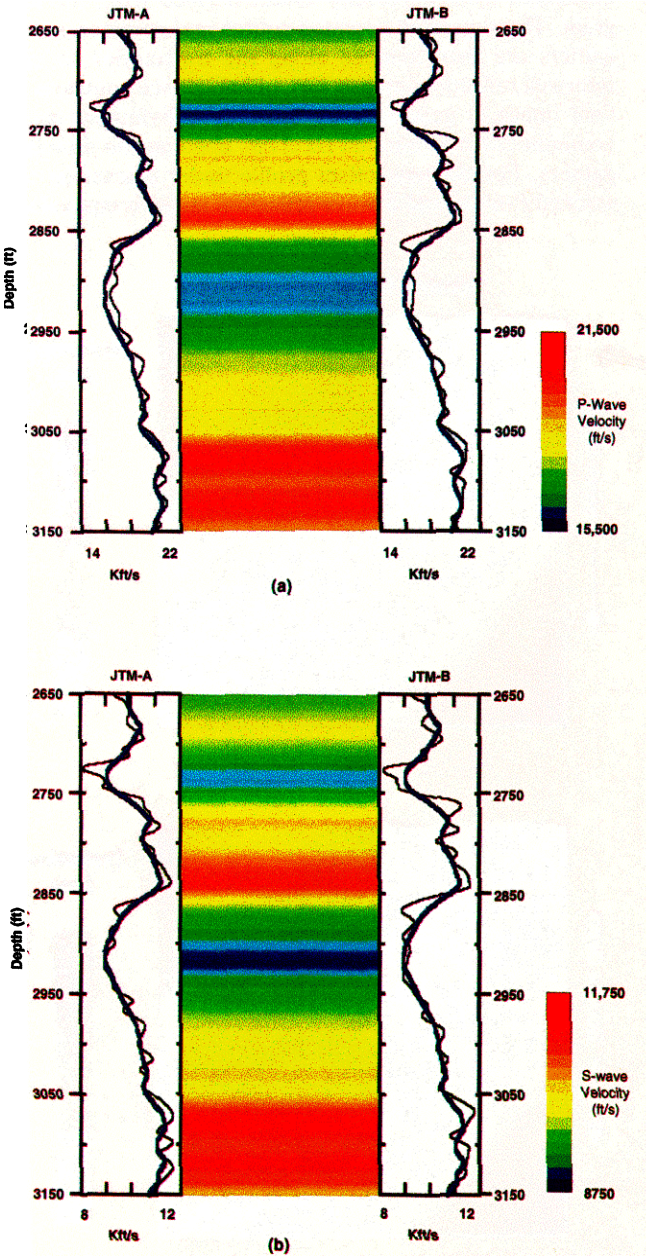

FIG. 7. These 1-D tomograms were produced from four ray trace iterations (with 10 backprojections each) of the STRINGS inversion: (a) P-wave velocity; (b) S-wave velocity. A vertical trace from the tomogram (wide blue line) is plotted with the smoothed sonic logs (thin lines) for comparison.

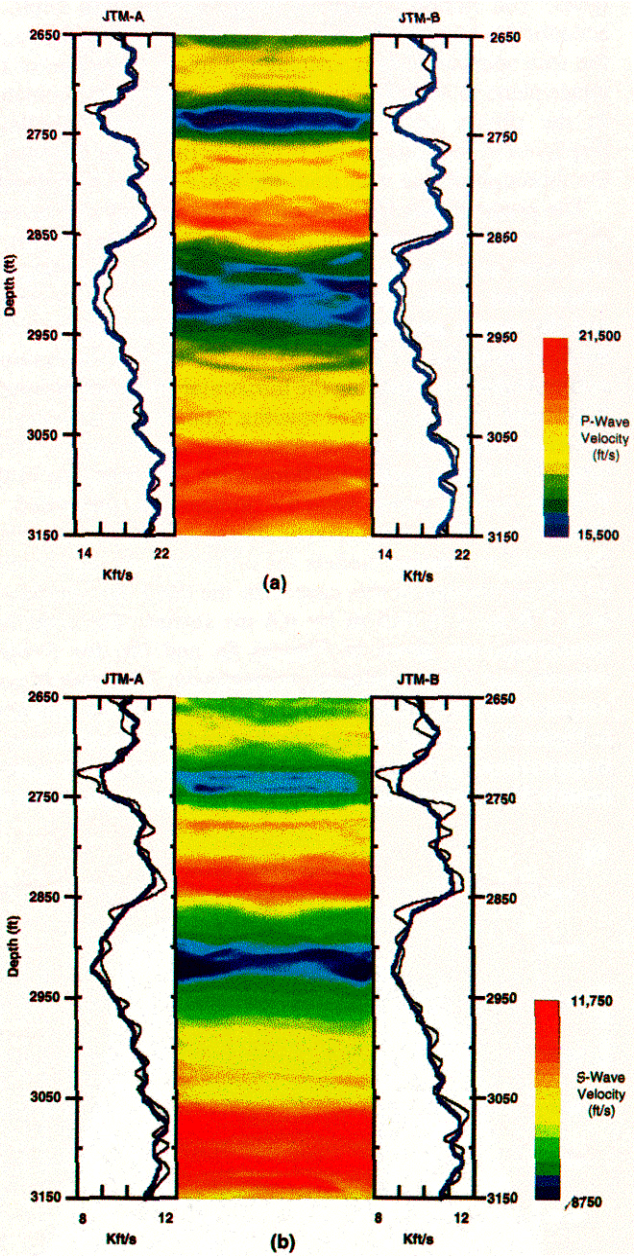

FIG. 8. These 2-D tomograms were produced after 80 backprojections of the STRINGS inversion: (a) P-wave velocity; (b) S-wave velocity. The small amplitude 2-D artifacts are a result of groups of traces with large traveltime residuals, perhaps caused by the mismatch between the calculated raypath and the actual raypath.

simple geological interpretation of the crosswell images. This is accomplished mostly by comparing the crosswell images with an interpretation of the well logs. We consider both the crosswell velocity tomogram and reflection impedance images. The images are oriented more-or-less east to west from source well to receiver well, (right to left, Figures 7, 8, and 10). To aid the description and interpretation of the crosswell images, sonic logs are plotted adjacent to each image. We begin with the velocity tomograms.

Velocity Tomograms

Traveltime tomography produces an image of velocity variations primarily associated with large-scale (> 1λ) heterogeneity and related to, among other things, lithology and porosity. In Figures 7 and 8, we have plotted the sonic logs from JTM-A and JTM-B and vertical traces from the tomograms alongside the color-coded tomograms. In these figures, the original logs (Figure 2) have been smoothed by a 10-foot sliding boxcar window. We see from the comparisons (Figure 7) that the vertical resolution of the tomogram is approximately 20-30 ft (6-9 m) for P-waves, or 1-1½ wavelengths at the mid-band frequency of 1000 Hz. For S-waves, the resolution is 10-15 ft (3-4 m) again 1-1½ wavelengths at the mid-band frequency. Despite its relatively low resolution in terms of wavelengths, the tomographic image has at least an order of magnitude better resolution than surface seismic data and provides an accurate estimate of velocity. These same statements can be made about the 2-D P-wave and S-wave tomograms shown in Figures 8a and 8b. However, there is an even better correlation between the logs and the vertical traces taken from the 2-D tomogram, indicating better resolution of heterogeneity, and that the 1-D tomogram is under parameterized.

Several prominent features are easily identified in the tomograms (Figures 7 and 8) and can be correlated with the logs. These include six major geological units or zones. The boundaries of these zones correlate very well with known markers defined from the well logs (Lemen et al., 1990). (See Figure 11.) From bottom to top these markers are:

1) Top of the San Andres formation at 3,050 ft (930 m).
2) Top of Grayburg M unit at 2,950 ft (899 m).
3) Top of Grayburg D5 unit at 2,860 ft (872 m).
4) Top of Grayburg Formation at about 2,750 ft (838 m).
5) Top of McElroy marker zone at 2,700 ft (823 m).

The D5 unit is the main reservoir zone and above the McElroy marker is the Queen formation. The low velocity zone from about 2,725 ft to 2,750 ft (830 to 838 m) corresponds with a low sonic velocity and high gamma-ray zone known from well logs near the top of the Grayburg formation. Also, the slower zone near 2750 ft corresponds with the Grayburg E marker, a gamma-ray peak, sonic-velocity low, and porosity peak. The transitions in velocity near 2,850 ft, 2,950 ft, and 3,050 ft all correlate with well-log markers for the D5 unit, M unit, and San Andres formation, respectively. The sharp transition in velocity from about 20,000 ft/s (6,096 m/s) above the primary pay zone to 16,500 ft/s (5,029 m/s) inside the pay zone near 2850 ft is verified with the sonic logs. Similarly, below the D5, the gradual transition out of the reservoir into faster rocks is accurately delineated. These features are easily correlated well-to-well with either the P-wave or the S-wave tomogram. The Grayburg-San Andres unconformity near 3050 ft is also resolved as an increase in both P-wave and S-wave velocities.

These large scale features, one or more wavelengths in vertical scale, are easily resolved by transmission tomogra-

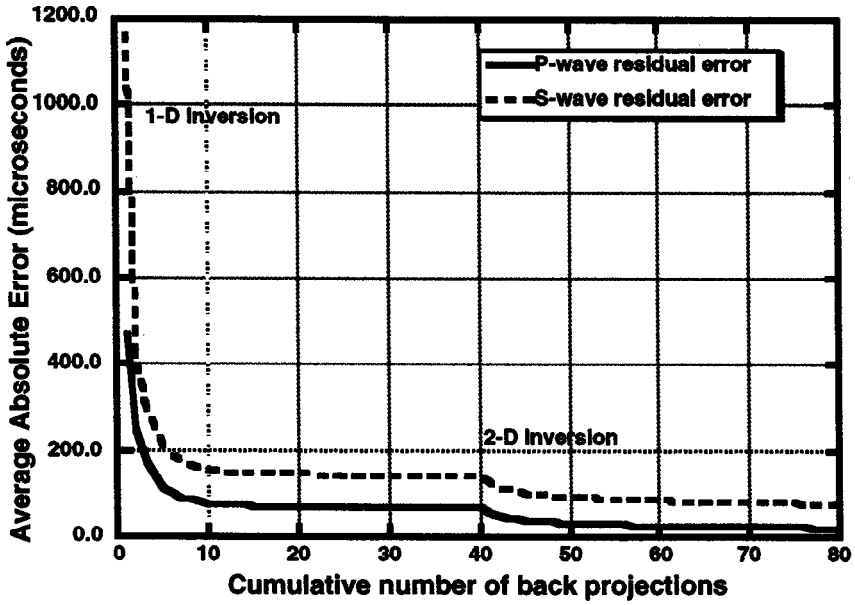

FIG. 9. Average absolute traveltime error for the 1-D and 2-D P-wave and S-wave tomograms. Although the residual values stabilize at about 20 microseconds for the P-waves and 50 microseconds for the S-waves, the tomograms continue to change as more iterations are run.

phy. And at this close well spacing, the tomogram is easily verified by the logs. As expected, however, vertical resolution from limited-view transmission tomography is better than lateral resolution. The 2-D tomogram has some unsightly artifacts related to the limited view. Although we see evidence of subtle lateral changes in the logs, such small scale variations are not resolved by transmission tomography, especially when they occur near the bottom or top of the profile where ray coverage is poorest. There are subtle lateral variations inside the reservoir zone indicated in the 2-D tomograms, but these too are difficult to interpret as geology for reasons we will now discuss.

Many of the 2-D velocity variations are small scale, at or below about 1% contrast to the surrounding rock. (See Figure 8.) They are more apparent in the tomograms because of the emphasis created by the particular color scale. Small scale variations such as these are extremely sensitive to many factors: 3-D wellbore geometry, experimental errors in the source-receiver locations, picking errors, model inconsistencies such as anisotropy, and mismatches between the assumed raypath and the actual raypath, as in the case of inverting head wave times along direct wave paths. For example, a 2% error in well spacing is only 5 ft (1 .5 m) for this profile and would introduce errors in the tomogram comparable and larger to some of the 2-D features seen in Figure 8.

The sensitivity to survey geometry can be seen as a problem, yet it can also be used as a quality control diagnostic during processing. That is, depth errors are known to create easily identified artifacts in the tomograms. This sensitivity to geometry allows one to correct depth errors much better than one can do with, say, independently recorded well logs from the two wells. And when the survey geometry is accurately known or corrected for, interwell velocity can be accurately estimated.

Finally, it would seem possible that the spatial variations imaged by tomography can be used to estimate reservoir properties (e.g., porosity), if the appropriate transformations are known, say, from core analysis (Nolen-Hoeksema et al., this issue). Indeed this is possible and is the subject of our continuing research. However, caution should be exercised when considering the small scale spatial variations and associated small magnitude variations in velocity of only a few percent. Tomograms are most reliable for large scale heterogeneities.

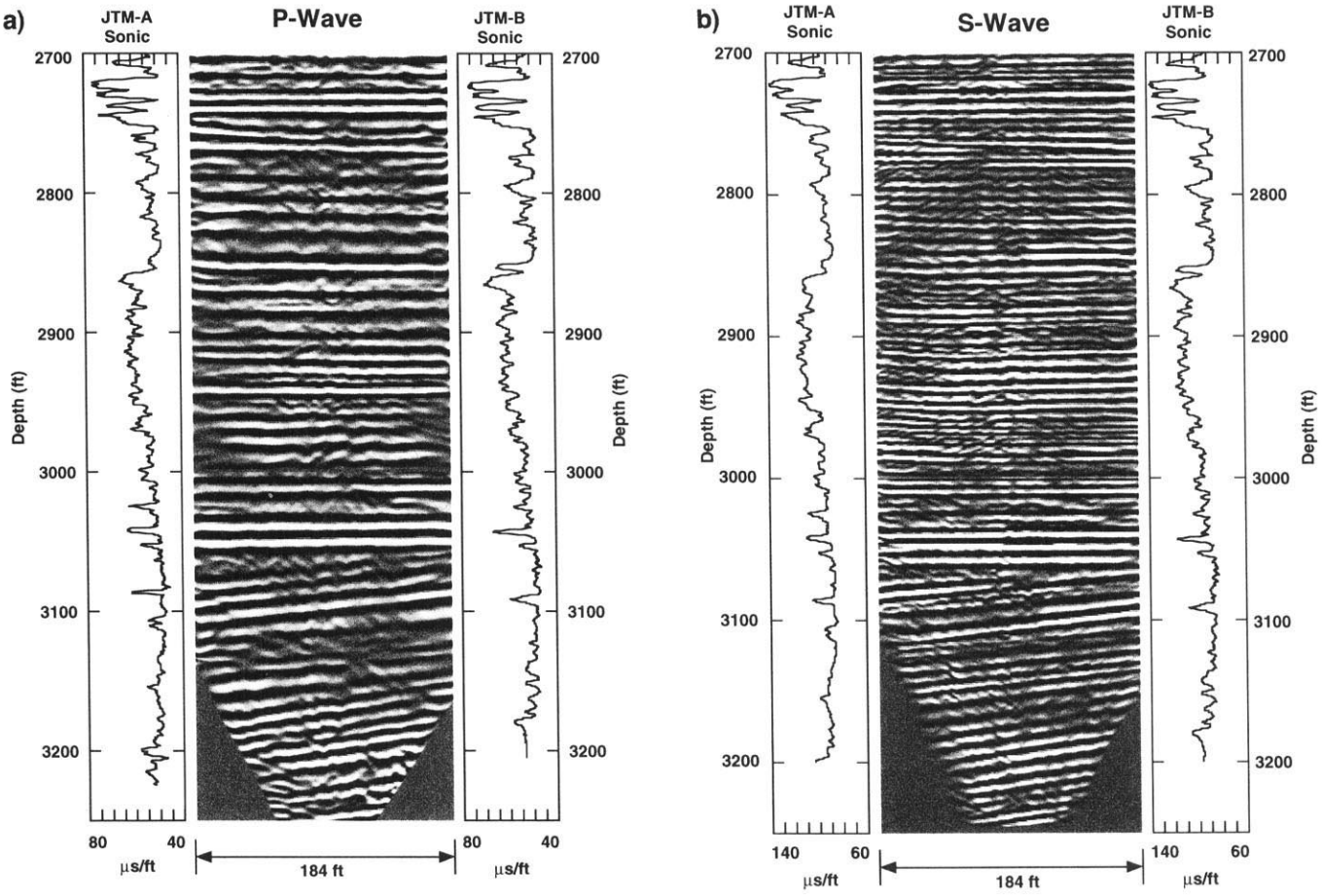

FIG. 10. Crosswell reflection images produced by VSP-CDP mapping: (a) P-to-P;(b) S-to-S. The reflection images have higher resolution than the tomogram and extend below the depth of the wellbore. Sonic logs are included for comparison.

Reflection Images

The P-wave and S-wave reflection images (Figures 10a and 10b, respectively) have 2-3 times better vertical resolution than the tomogram and add complementary small scale detail to the tomogram. At this time, however, the reflection images are strictly qualitative "pictures" and interpretable in terms of only the geometry of the impedance boundaries generating the reflection events. Nevertheless, this information is extremely valuable for it represents the geometry of the structures for reservoir delineation purposes. Again, just as we did with the tomograms, we must take care in interpreting the reflection images as well, in this case the amplitudes. These images are not zero-offset seismic sections of the type produced from surface seismic data. They are generated from angles ranging from about 20" to 70" above grazing. At such steep angles, the Fresnel zone contributing to the reflection event may be quite large, resulting in significant loss in lateral resolution. Even with these caveats, the horizons generated by reflection imaging correlate remarkably well with the major log markers discussed above and also with the velocity transitions seen in the tomogram. There is also the fine-scale vertical detail not seen in the tomograms.

The first example we discuss comes from within the main pay, the Grayburg D5 unit, where several reflection events, some with obvious and subtle variations in character, can be seen. Many of these events carry across from well to well and thus may correspond to continuous reservoir horizons or zones. A second example is found between 2,750 and 2,775 ft, where the Grayburg E marker at about 2750 ft can be carried well-to-well using the reflection images. A small pinchout can be seen near the top of the Grayburg E unit. The lateral variation indicated by this pinchout is suggested by the well logs, where the reflector corresponding to the sonic-velocity low at 2,760 ft in the receiver well appears to pinchout or downlap near the Grayburg E marker. This range of depths corresponds to the relatively slow zone in the tomogram.

Perhaps the most striking feature of the reflection image occurs near 3,050 ft, the boundary between the San Andres and Grayburg formations. The strata above this depth are mostly horizontal, whereas below the strata are slightly dipping from right to left. Both P-wave (Figure 10a) and S-wave (Figure 10b) reflection images show this ***angular*** unconformity. San Andres strata dip from west to east toward the Midland Basin, while the overlying Grayburg strata are flat. This boundary is known to be an unconformity (Harris et al., 1984; Walker and Harris, 1986) corresponding to a regression or low stand of sea-level that exposed the underlying San Andres carbonate platform. The reflection images reveal that the reflector corresponding to the sonic-velocity low (gamma-ray peak) at 3,080 ft at the receiver well terminates up dip at the unconformity near the source well. The reflector corresponding to the sonic-velocity low (gamma-ray peak) at 3,100 ft at the receiver well ties to the 3,080-foot velocity low in the source well. This dipping feature is easily identified with the reflection image and cannot be resolved from surface seismic or for that matter using the tomogram, but only with the crosswell reflection images. Moreover, the dip would not have been interpreted as such from the logs alone.

It is clear that vertical resolution from reflections is 2-3 times better than transmission tomography, easily less than 10 ft (3 m) for P-waves and better than 5 ft (1.5 m) for S-waves. This detail cannot be matched by surface seismic or vertical seismic profiles. However, lateral resolution for the reflection is not as good (Lazaratos et al., this issue). There are also subtle variations in reflection character within the five major geologic units that may be more amenable to depositional model analysis (Mitchum et al., 1977) than even the logs. The fine vertical scale features may correspond to depositional sequence boundaries caused by sea-level changes at a scale of only a few feet. Furthermore, the 2-D pattern of the heterogeneity seen in the reflection images appears to vary from zone to zone. These patterns may be indicative of changes in depositional rate or small scale sea level fluctuations heretofore not seen with surface seismic methods.

Core Analysis

The other major objective of the project was to determine whether crosswell seismic profiling can be used to monitor changes in CO_2 saturation. Results of the core study would of course be useful in support of reservoir characterization as well. We already have velocity tomograms and the reflection images that form the baseline for comparison with images to be produced after CO_2 injection. To assess the potential for successful monitoring, we must estimate the expected contrast in seismic properties, namely velocity and density, caused by injected CO_2. We summarize here the results of reservoir quality analyses run on full diameter cores and the geophysical analyses performed on 20 core plugs. Details are given by Nolen-Hoeksema et al. (this issue).

A total of 285 ft (87 m) of 3.25-inch diameter, unoriented core was cut from the observation well (JTM-A) between 2,775 ft and 3,060 ft (846-933 m), i.e., through the Grayburg and into the San Andres. Routine core analysis, run on 285 full-diameter cores, included measurements of porosity, air permeability, and grain density. Porosity ranges from 0.8% to 21.1% and averages 7.4%. Permeability ranges from 0.01 md to 217 md and averages 6.2 md. Grain density ranges from 2.69 to 2.89 g/cm^3 and averages 2.80 g/cm^3. These measurements are consistent with the presurvey estimates and indicate the large variability in reservoir quality known to exist throughout the field.

In addition to the routine core study, 20 1.5-inch diameter plugs were selected for ultrasonic velocity analysis. Porosity, permeability, and density were also measured on these 20 plugs. Compressional and shear velocities were recorded at four differential pressures ($P_{diff} = P_{confining} - P_{pore}$). The measurements at 2000 psid (13.8 MPa) are of primary interest because they correspond to reservoir conditions. The measured data for P- and S-wave velocities and porosity are presented in Figure 11. The measured results show that P-wave velocities are increased by 4.26% on average when air is replaced with reservoir brine. As expected, the measurements also show that S-wave velocities are relatively insensitive (~-0.65%) to changes in fluid saturation.

Gassmann's equation was used to model (at low frequencies) the dry and brine-saturated velocity data. Using the mineral moduli estimated from the grain density measurements, we then matched the P-wave and S-wave sonic logs from the well with synthetic logs calculated from the Gassmann model. After obtaining a satisfactory match to the sonic logs, Gassmann's model was used again to estimate the effects of CO_2 flooding on the velocities and densities of the Grayburg formation.

At reservoir pressures and temperatures, the P-wave velocity of CO_2 is approximately 200 m/s, whereas oil is approximately 1400 m/s. Also, the density of CO_2 is very sensitive to pressure, especially near miscibility and near the critical point at 1070 psia, though it is always less than light oil (-0.87 g/cm^3). At reservoir pressures of 900 to 1200 psig, the density of CO_2 varies from about 0.2 g/cm^3 to about 0.7 g/cm^3. Although these contrasts in the properties of the fluids are significant, the bulk contrast sensed by seismic **waves** depends on the saturation and mixture ratios of oil, water, and CO_2 in the pore space. Therefore the Gassmann calculations were made for a measured pre-CO_2 water-to-oil ratio of 53%-47% and an anticipated post-CO_2 water-oil-gas immiscible ratio of 16%-8%-76%.

The results indicate that the P-wave velocity in a CO_2-swept zone decreases about 2% from that of an unswept zone. The decrease in the P-wave to S-wave velocity ratio is slightly larger at about 2.5%. The contrast is better for bulk-wave velocity and bulk-wave impedance, averaging 3.7% and 4.8%, respectively. Nolen-Hoeksema et al. (this issue) provide more details on these estimates.

DISCUSSION

The P-wave velocity tomogram and reflection image are plotted together with the suite of logs in Figure 12. The color display of the tomogram is overlaid by the reflection image for easy comparison. The tomogram provides quantitative information on larger-scale features and is suitable for quantitative estimation of reservoir properties such as porosity. Reflection images, though qualitative, provide information on smaller scale heterogeneity. In addition, the reflection images provide a direct delineation of stratigraphic continuity, including small scale features inside the reservoir pay zone. On the basis of these results, it is clear that crosswell profiling is capable of high-resolution reservoir delineation. The relationship between velocity and porosity given by the core analysis (Figure 11) provides a basis for both deterministic and statistical estimation of porosity from the tomogram. While neither velocity tomograms or reflection images directly give flow permeability, the images may be used for interpolating permeability estimates made at the wellbores into the region between wells. Research on estimating permeability using regression fits and geostatistical methods is underway and will be reported at a later date. Bashore et al. (1995) have conducted a proof-of-concept study using these crosswell data and they have demonstrated their potential utility in building improved reservoir models for flow simulations.

Crosswell images provide complementary information to logs and surface seismic sections. That is, crosswell seismic profiling fills the gap in coverage and resolution between logs and surface seismic images. This unique strength of the method is illustrated in Figure 13 with a 2-D surface seismic section from the study area, the crosswell reflection image plotted with the velocity tomogram, the sonic log, and ultrasonic core samples from the observation well. The wavelength of surface seismic (10-80 Hz) at reservoir depth is approximately 300 ft (91 m); therefore, the entire 100-foot (30-m) thick pay zone is less than one-third wavelength. It is

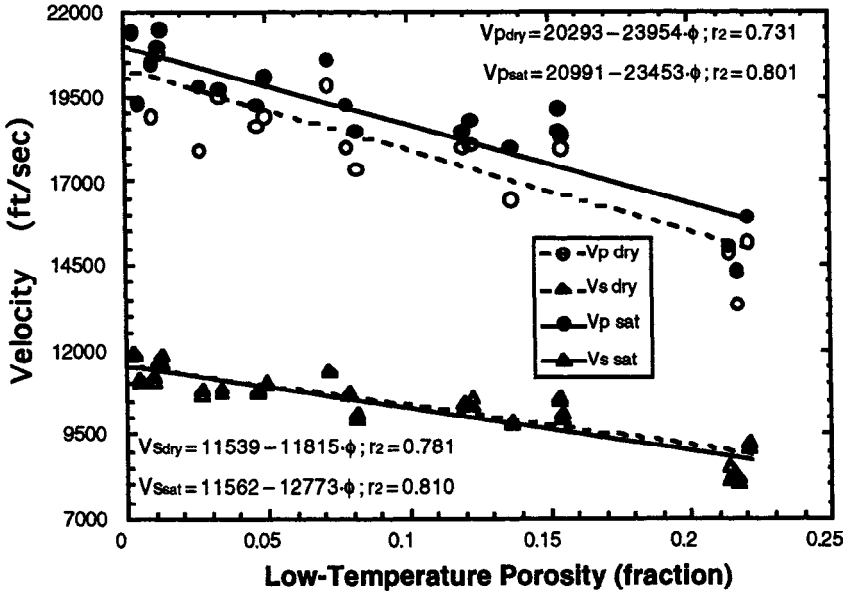

FIG. 11. Measured values of P-wave and S-wave velocity are plotted versus measured porosity for 20 dry and saturated core plugs from the Grayburg and San Andres formations. P-wave velocity increases an average of 4.26% when saturated with reservoir brine. S-waves are relatively insensitive to fluid saturation.

clear that the pay zone interval cannot be resolved by surface-based seismic methods. Furthermore, the internal structure of the pay zone (features on the order of 10 ft (3 m) thick) would not be resolved from surface seismic data with twice the bandwidth. Clearly, crosswell seismic profiles, whether tomography or reflections, offer complementary high-resolution advantages to surface seismic profiles. And, unlike surface seismic images, crosswell images are presented as true depth sections (not time sections), thus removing the time-to-depth ambiguity associated with velocity in surface seismic data.

It is a mistake to think that one or the other of the two crosswell images is less important. Note in the reflection images how the absence of low frequencies makes it difficult to interpret the many cycles of the reflection events with the depositional system suggested by the low-frequency trends of the logs. This missing bandwidth is provided by the velocity tomogram as illustrated in Figure 12 or Figure 13. Also illustrated in these figures is the failure of transmission tomography to "resolve" the dip of the beds below the unconformity near the bottom of the profile, though it does give a hint of the dip and, of course, the velocity variation at the transition. The dip information is provided by the reflection image. This complementary nature of the tomographic velocity and reflection images is very important for interpreting multiscale heterogeneous reservoirs.

As for monitoring, our P-wave tomography results indicate that velocity changes greater than about 1% may be reliably imaged using differential tomography. Though not presented here, we have run a second repeat crosswell survey at the site and determined that the survey can be repeated to better than 1% accuracy; therefore, changes in P-wave velocity and Poisson's ratio of a few percent or more associated with injected CO_2 are expected to be visible with crosswell seismic profiling. Furthermore, changes in P-wave and S-wave impedance associated with decreases in both velocity and density may be visible on differential reflection sections.

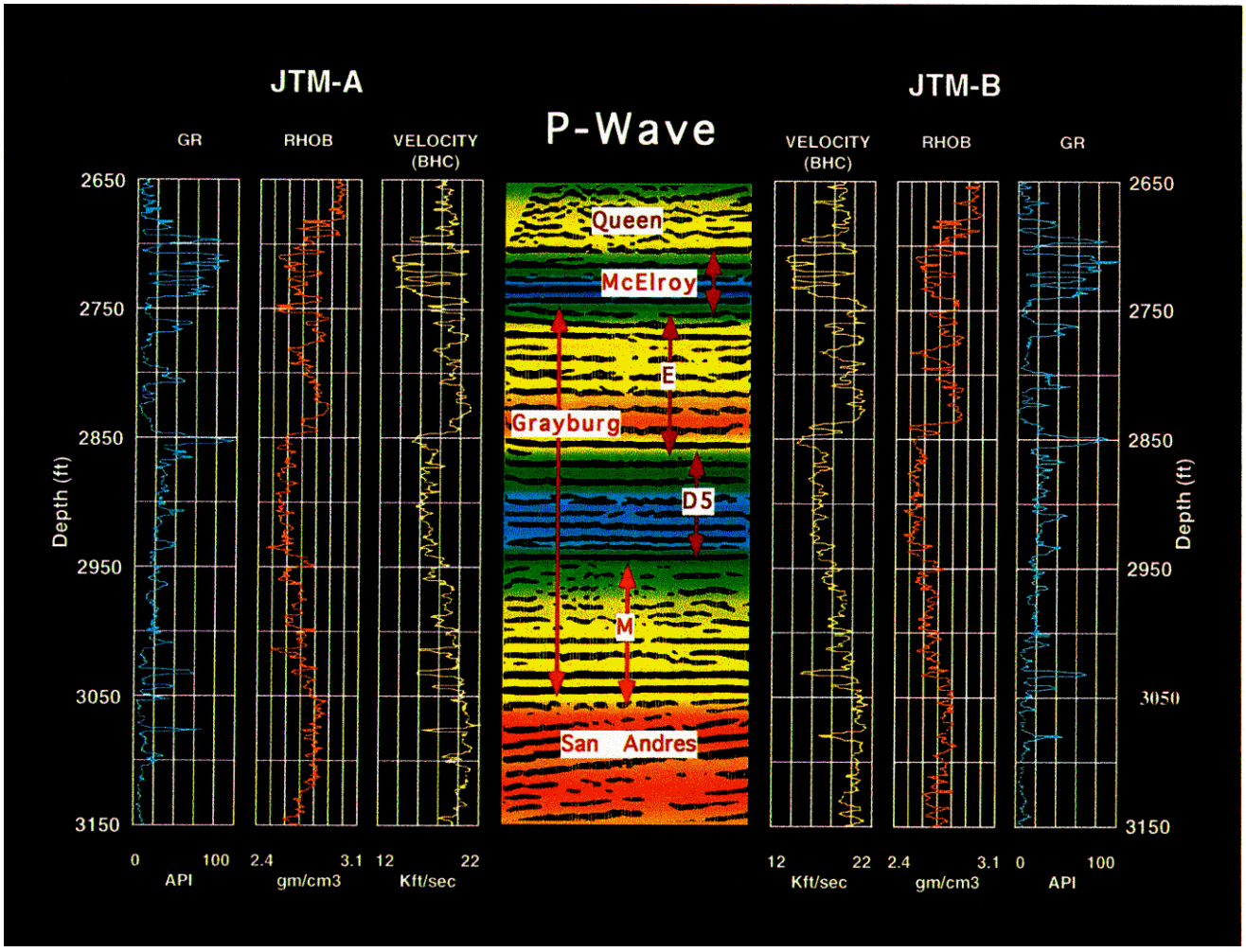

FIG. 12. The 1-D P-wave tomogram overlain by the P-wave reflection image is displayed with the suite of well logs for correlation and interpretation. Six major geological zones are delineated in the velocity image. Within these zones are many reflecting horizons, perhaps corresponding to depositional sequence boundaries.

CONCLUSIONS

One role for crosswell seismic profiling is to complement the low-resolution but large coverage available from 3-D surface seismic profiles and the high-resolution but low coverage provided by well logs. We have seen how this is done for a CO_2 pilot site in west Texas. Crosswell transmission traveltimes and reflections are combined to image the internal structure of the reservoir. The high-resolution nature of the images is a result of the cooperation between a new data acquisition technique of shooting on-the-fly and reflection data processing. Though at close well spacing, only 184 ft (56 m) between wells for Profile #1, our results illustrate the enormous potential of crosswell seismic profiles to address reservoir delineation and characterization problems usefully. These first results for Profile #1 provide encouraging clues into the potential of crosswell technology. Stratigraphic analysis at scales of only a few meters at depths of several thousands of meters may provide new insight into reservoir analysis and geological processes.

There are several areas of future research planned. Porosity and permeability cross-sections are being generated from both deterministic and geostatistical methods, for use in fluid flow simulations as part of the CO_2 pilot study. In addition, our plans include using logs, cores, and an anticipated 3-D surface survey to make quantitative estimates of reservoir properties throughout the field, not just in the pilot area. The crosswell data are also being imaged with migration algorithms and diffraction tomography (Mo and Harris, 1993; Harris and Wang, 1993). Another set of pre-CO_2 crosswell profiles (and several offset VSPs) has already been recorded to verify repeatability of the field experiment. Post-CO_2 injection profiles (and VSPs) are planned for monitoring. On the basis of these results, we believe crosswell methods will be extremely useful in both reservoir delineation, reservoir characterization, and CO_2 monitoring.

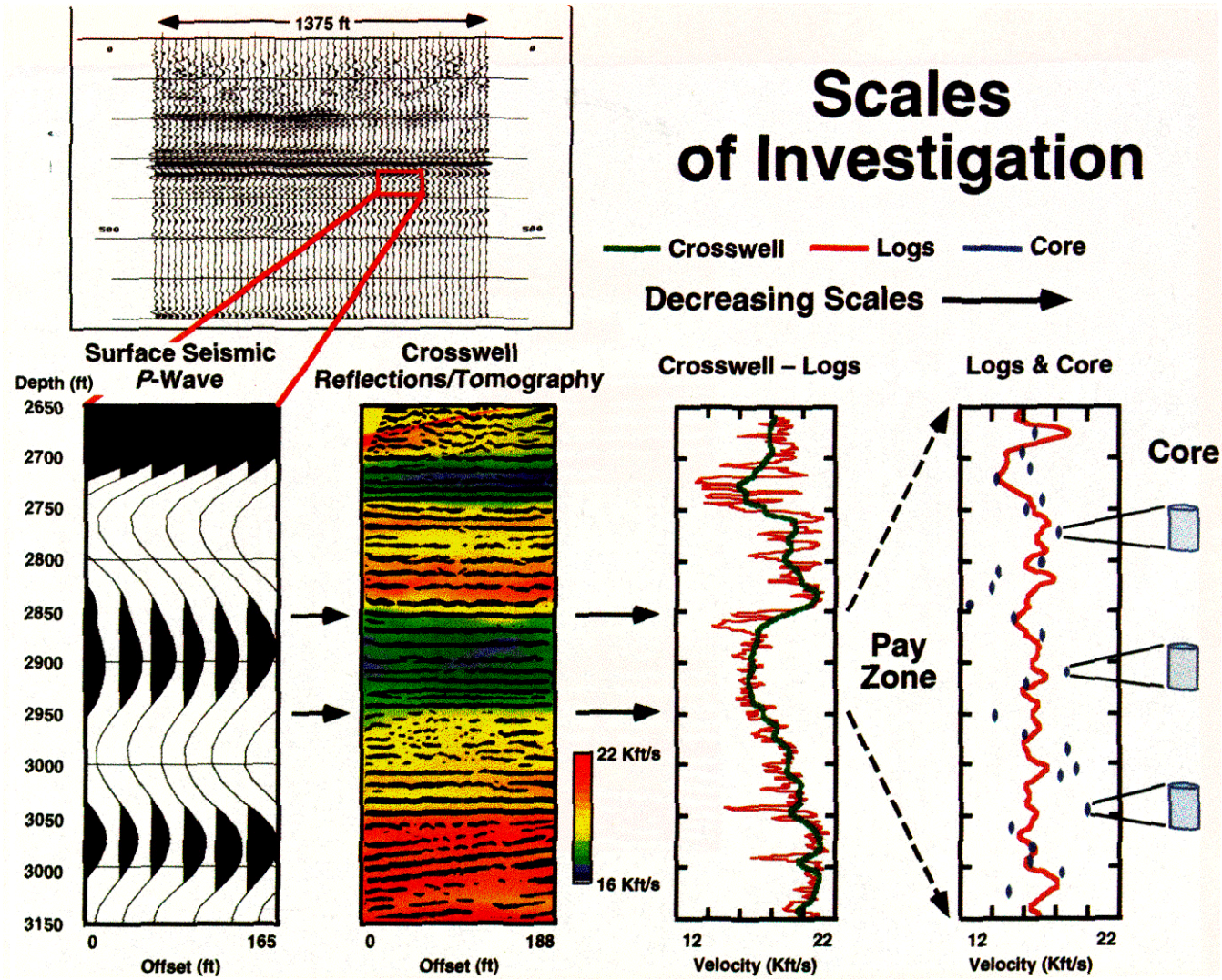

FIG. 13. Seismic methods span a range of frequencies and sample a range of scales. Here we show how crosswell methods are used to fill a gap between the low resolution and large coverage of surface seismic and the high resolution and low coverage of logs and core.

ACKNOWLEDGMENTS

The authors thank Chevron Petroleum Technology Company and Chevron USA, Inc. for sponsoring this project and making available the field site. Special thanks to Bjorn Paulsson for initiating the project and to Ronnie Brumfield of Chevron USA for his help in executing the field work. We also thank the Gas Research Institute, the Packard Foundation, and the industrial sponsors of Stanford's Seismic Tomography Project for their continuing support.

REFERENCES

Bashore, W. M., Langan, R. T., Tucker, K. E., and Griffith, P. J., 1995, Geostatistical integration of crosswell data for carbonate reservoir modeling, McElroy Field, Texas: in Stoudt, E. L. and Harris, P. M., Eds., Hydrocarbon reservoir characterization-Geologic framework and flow unit modeling: SEPM Short Course No. 34, SEPM, 199-226.

Harris, P. M., Dodman, C. A., and Bliefnick, D. M., 1984, Permian (Guadalupian) reservoir facies, McElroy Field, west Texas: in Carbonate Sands-A core workshop, Harris, P. M. Ed., SEPM Core Workshop No. 5, 136-174.

Harris, J. M., 88, High frequency cross-well seismic measurements in sedimentary rocks, 58th Ann. Intemat. Mtg., Soc. Expl. Geophys., Expanded Abstracts, pp. 147-150.

Harris, J. M., Lazaratos, S. K., and Michelena, R., 1990. Tomographic strmg inversion, 60th Ann. Internat. Mtg., Soc. Expl. Geophys., 84-88.

Harris, J. M. and Wang, G. Y., 1993, Diffraction tomography for inhomogeneities in a layered background medium, 63rd Ann. Internat. Mtg., Soc. Expl. Geophys., Expanded Abstracts, 49-52.

Lazaratos, S., Harris, J. M., Rector, J. W. and Van Schaack, M., 1995, High-resolution crosswell imaging of a west Texas carbonate reservoir: Part "Reflection imaging, Geophysics, 60,702-711.

Lemen, M. A., Burlas, T. C., and Roe, L. M., 1990, Waterflood pattern realignment at the McElroy field-Section 205 case history: *SPE Paper* 20120 presented at the 1990 Permian Basin Oil & Gas Recovery Conference, Midland, Texas, March 8-9.

Mitchum, R. M., Jr., Vail, P. R., and Thompson, S., III, 1977, Seismic stratigraphy and global changes of sea level, Part 2, The depositional sequence as a basic unit for stratigraphic analysis: in Seismic Stratigraphy-Applications to Hydrocarbon Exploration, AAPG Memoir 26, 53-62.

MO, Le-Wei and Harris, J. M. 1993, Migration of cross-well seismic data, 63rd Ann. Internat. Mtg., Soc. Expl. Geophys., Expanded Abstracts, 317-320.

Nolen-Hoeksema, R. C., Zhijing Wang, Harris, J. M., and Langan, R. T. 1995. High-resolution crosswell imaging of a west Texas carbonate reservoir: Part 5-Core Analysis, Geophysics, 60, 712-726.

Rector, J., S. Lazaratos, Harris J. M., and Van Schaack, M., 1995. High-resolution crosswell imaging of a west Texas carbonate reservoir: Part 3-Wavefield separation of reflections, Geophysics, *60,* 692-701.

Van Schaack, M., Harris, J. M., Rector, J. W. and Lazaratos, S., 1995, High-resolution crosswell imaging of a west Texas carbonate reservoir: Part 2-Wavefield modeling and analysis, Geophysics, 60, 682-691.

Walker, S. D., and Harris, P. M., 1986, McElroy Field-Development of a dolomite reservoir, Permian Basin of west Texas: Permian Basin/SEPM Publication, 86-26, 127-132.

Ward, R. F., Kendall, C. G. St. C., and Harris, P. M., 1986, Upper Permian (Guadalupian) facies and their association with hydrocarbons-Permian Basin, west Texas and New Mexico: AAPG Bulletin, 70 (3), 239-262.